Sensing and Bio-Sensing Research 43 (2024) 100603

Contents lists available at ScienceDirect

Sensing and Bio-Sensing Research

journal homepage: www.elsevier.com/locate/sbsr

Graphene based Mo_6 cluster hybrid for detecting simulant nerve agent DMMP

Juan Casanova-Chafer [a,b,*], Xavier Blanch [b], Ana Moreno [c], Rocio Garcia-Aboal [c], Pedro Atienzar [c], Eduard Llobet [b], Marta Feliz [c,**]

[a] ChIPS Research Group, Department of Chemistry, Université de Mons, 7000 Mons, Belgium
[b] MINOS Research Group, Department of Electronics Engineering, Universitat Rovira i Virgili, 43007 Tarragona, Spain
[c] Instituto de Tecnología Química, Universitat Politècnica de València - Consejo Superior de Investigaciones Científicas (UPV-CSIC), 46022 Valencia, Spain

ARTICLE INFO

Keywords:
Graphene
Mo_6 cluster
DMMP
Nerve agent
Trace levels

ABSTRACT

Nerve agents are highly toxic chemical compounds that pose significant threats to human health and safety. Detecting and identifying these agents quickly is crucial for preventing their exposure and providing timely treatment. This study proposes the use of nanohybrids comprising crystalline octahedral molybdenum iodide cluster material supported on graphene (Mo_6@Graphene) as a novel sensing material for the detection of dimethyl methylphosphonate (DMMP), a simulant of sarin nerve agent. The electrical sensing performance towards different concentrations of DMMP and at room temperature demonstrated fast and sensitive responses to DMMP, with almost full recovery of the sensor baseline in a few minutes. The calibration curve obtained showed a linear relationship between the sensor response and DMMP concentration, enabling the estimation of the limit of detection (LOD) of 270 ppb. The robustness of the Mo_6@Graphene nanomaterial towards DMMP was assessed using various techniques, including Raman spectroscopy, X-ray diffraction and photoelectron spectroscopy. The binding energies (BEs) between DMMP and the supported Mo_6 clusters determined by DFT calculations revealed H-bonding interactions involved in the sensing mechanism. The excellent sensing performance of the Mo_6@Graphene film, combined with its low power consumption and high stability, makes it a promising candidate for the detection of nerve agents and their simulants.

1. Introduction

Nerve agents are a class of toxic chemical compounds that cause severe harm to humans and other living organisms, and have been used as weapons of mass destruction or as a tool for assassination. These agents are designed to interfere with the normal functioning of the nervous system, leading to a range of symptoms that can include seizures, respiratory distress, and ultimately death [1]. The history of nerve agents dates back to the early 20th century, with the development of organophosphate compounds as insecticides [2]. However, it was not until World War II that nerve agents were weaponized for use in warfare [3]. After the war, the use of nerve agents continued, for instance, the Japanese doomsday cult Aum Shinrikyo used the nerve agent sarin ($C_4H_{10}FO_2P$) in a terrorist attack on the Tokyo subway system in 1995 [4]. The use of nerve agents as a weapon of mass destruction and the vulnerability of indoor infrastructures exposed to chemical terrorist attacks pose a significant point of concern for authorities responsible for incident preparedness and prevention. This relates to the specific features of indoor spaces and their extremely high population exposure potential, given the current organization of society. The range of possibilities for terrorist attacks involving toxic chemicals is wide. In any event, an attack using unconventional weapons would certainly cause serious economic and social disruption to normal, day-to-day activities. In all areas of countermeasures against warfare agent attacks, be it threat assessment, prevention, preparedness, response or recovery it is crucial to be able to detect and, if possible, identify the threatening material. The timeline for perceiving the attack and setting an alarm for evacuating the building would take several minutes and result in many casualties. Thus, the existence of early warning detection systems is critical for preventing casualties, as detecting nerve agents quickly is

* Corresponding author at: ChIPS Research Group, Department of Chemistry, Université de Mons, 7000 Mons, Belgium.
** Corresponding author at: Instituto de Tecnología Química, Universitat Politècnica de València - Consejo Superior de Investigaciones Científicas (UPV-CSIC), Avd. de los Naranjos s/n, 46022 Valencia, Spain.
E-mail addresses: juan.casanovachafer@umons.ac.be (J. Casanova-Chafer), mfeliz@itq.upv.es (M. Feliz).

https://doi.org/10.1016/j.sbsr.2023.100603
Received 18 August 2023; Received in revised form 27 October 2023; Accepted 13 November 2023
Available online 14 November 2023

crucial to prevent their use and provide treatment to those who may have been exposed. However, the use of sarin gas in laboratory settings poses significant risks. Dimethyl methylphosphonate (DMMP) is another class of organophosphorus compound used as a simulant of sarin gas for chemical defense training and laboratory testing. DMMP is moderately toxic, causing irritation to the eyes, skin, and respiratory system, and nausea, vomiting, and headaches if inhaled in large amounts [5]. One of the key properties of DMMP is its high volatility [6], which is useful for gas phase detection. The implementation of gas sensors is an essential tool for the detection of organophosphorus compounds by real-time monitoring and data collection. The accuracy and precision of measurements can be improved by using data from multiple sensors over a wide area, providing a comprehensive picture of potentially dangerous situations [7]. Besides, developing extended sensing networks would enable a better decision-making based on the information gathered [8]. Within the different types of gas sensors, chemoresistive sensors have attracted great attention as they offer high sensitivity, low cost, ease of fabrication, real-time monitoring, and rapid detection [9]. These chemical devices are based on the interaction between the nerve agent (or the simulant compound) and a sensitive film, resulting in variations in the electrical conductivity of the nanomaterial. However, effective detection may be subject to interference from other chemicals or environmental factors.

Different types of nanomaterials such as metal oxides, dichalcogenides, polymers and carbon derivatives have been used to detect DMMP [10,11]. However, graphene has emerged as a promising option due to its outstanding properties, such as high surface-to-volume ratio, high carrier mobility, and ability to work under room temperature conditions [12]. Graphene-based gas sensors are suitable for developing extended sensing networks due to their low power consumption, inexpensiveness, and long-term stability [13]. However, pristine graphene is limited by poor specificity and selectivity towards gas compounds due to its sp^2 configuration. Therefore, graphene hybrids are required to enhance sensitivity and specificity to detect low amounts of nerve agents. For instance, Z. Yang et al. have developed a hybrid comprising polypyrrole and reduced graphene oxide (rGO) to detect 5 ppm of DMMP [14], while S. Xu et al. have developed a surface acoustic wave (SAW) sensor based on graphene/PVDF (polyvinylidene fluoride) for detecting up to 10 ppm of the target gas [15].

The materials composed of nanometer-sized octahedral molybdenum clusters (< 2 nm) are emerging materials in the field of gas sensing purposes [16]. These $[Mo_6L^i_8L^a_6]$ cluster units are robust entities composed of inner halide ligands (L^i) and organic or inorganic apical (or terminal) ligands (L^a). Mo_6 clusters act as powerful photosensitizers and are also efficient luminophores that, under photoactivation, either exhibit phosphorescence in the 550–900 nm window or reacts with oxygen to provide singlet molecular oxygen ($^1O_2$). Until now, the existing literature on analyte gas sensing using Mo_6 cluster-based nanomaterials was mostly explored as optical oxygen sensors [17–21], and the detection of environmental humidity was also explored [22]. More recently, a crystalline material composed of Mo_6 clusters with iodides was deposited onto graphene layers resulting in orthogonal sensors to NH_3 and NO_2 gases [23], and a Mo_6/MoS_2 nanocomposite showed ammonia detection performance [24]. Until present, and to the best of our knowledge, the use of clusters to detect nerve agents and their simulants remains totally unexplored. In this work, the use of Mo_6 cluster-based crystalline material supported on graphene is proposed, for the first time, to detect DMMP. The integration of this nanohybrid into a resistive transduction scheme has demonstrated its potential to detect typical gas pollutants, such as NO_2 [23].

2. Experimental section

2.1. Materials

DMMP was obtained from commercial resources (VICI Metronics Inc.). The crystalline $[Mo_6I^i_8(OH)^a_4(H_2O)^a_2]\cdot 2H_2O$ (Mo_6) material and its derived nanohybrid (Mo_6@Graphene) were prepared by our recently reported procedures [23]. The Mo_6@Graphene composition and stability after DMMP exposure were analyzed by FT-IR (Fig. S1), powder X-Ray Diffraction (XRD) (Fig. S2a) and Raman spectroscopy (Fig. S2b). For textural analyses, Fig. S3 and S4 were recorded by Field-Emission Scanning Electron Microscopy (FESEM) and High-Resolution Transmission Electron Microscopy (HR-TEM), respectively. The sensing device was fabricated by depositing the resulting nanohybrid onto an alumina substrate using the spray-coating technique. The substrate includes a platinum screen-printed electrode.

2.2. Characterization techniques

FT-IR spectra were measured on KBr pellets with a Nicolet 8700 Thermo spectrometer. The Raman spectra were obtained from solid samples previously deposited onto glass substrates, using a “Reflex” Renishaw spectrometer, equipped with an Olympus microscope. The exciting wavelength was 514 nm of an Ar^+ ion laser while the laser power was ~10–25 mW; 20 acquisitions were taken for each spectrum. Powder X-ray diffraction patterns were obtained by using a Philips X’Pert diffractometer and copper radiation (CuKα = 1.541178 Å). FESEM images were recorded with a Zeiss Ultra 55 field FESEM apparatus (Atlanta, GA, USA) equipped with a back-scattered electron (BSE) detector. Samples for HR-TEM were deposited onto carbon-coated copper grids. HR-TEM images were recorded by using a JEOL JEM2100F microscope operating at 200 kV. X-ray photoelectron (XPS) spectra were collected from solid samples previously deposited onto Cu substrates, using a SPECS spectrometer with a 150MCD-9 detector and a non-monochromatic AlKα (1486.6 eV) X-ray source. Spectra were recorded using an analyzer pass energy of 30 eV, an X-ray power of 100 W and under an operating pressure of 10^{-9} mbar. During data processing of the XPS spectra, BE values were referenced to the C1s peak (284.5 eV). Spectra treatment has been performed using the CASA software.

2.3. Computational details

The calculations were conducted with the Gaussian 09 program suite. Density functional theory was applied with the PBE0 functional [25,26]. Relativistic electron core potentials (RECP) from the Stuttgart group and its associated basis sets (SDDALL) [27] were used to represent the molybdenum [28] and the iodine atoms [29] and augmented, in the case of Mo, by an f polarization function (Mo: α = 1.043) [30] and in the case of the I, with a d polarization function (I: α = 0.289) [31]. The 6-31G(d,p) basis set was used to represent the remaining atoms (O, N, and H) of the molecular systems. The geometry optimizations were performed in the gas phase without any symmetry constraint followed by analytical frequency calculations to confirm that a minimum has been reached. Zero-point energies were included in binding energy (BE) calculations, and the BEs were calculated using $BE = E_{(cluster\text{-}DMMP)} - [E_{cluster} + E_{DMMP}]$. The *trans*-$[Mo_6I^i_8(OH)^a_4(H_2O)^a_2]$ cluster was built as a representative model for DMMP adsorption sites, considering that water and hydroxo positioning around the octahedral metal framework cannot be inferred from the X-ray diffraction structure. The guess geometries of the gas-cluster adduct were raised considering a random positioning of the DMMP analyte concerning all the cluster ligands (water, hydroxo, and iodide) of the cluster model.

2.4. Experimental set-up and sensing measurements

In the laboratory, a system was employed for the measurement of DMMP that involved the generation of varying concentrations of the gas by the application of synthetic air. The system comprised two distinct mass flows, to which synthetic air (Air Premier Purity: 99.995%) was applied directly from a calibrated bottle. One of these mass flows

incorporated a Permeation System, which comprised a stainless-steel tube covered with a heated belt. The entire permeation system was connected to a PID controller (proportional integral derivative), which stabilized the temperature inside the tube. At the end of the system, another mass flow controller was implemented to facilitate dissolution with the synthetic air-controlled mass flow. Fig. 1 depicts a diagram of the system employed. The system utilized a Teflon airtight sensing chamber, in which a mixture of gas concentration generated and synthetic air was introduced. Resistance changes induced in the sensors were monitored using an Agilent HP 34972 A multimeter. The resistance value of the sensitive film has been recorded every second.

The permeation system's internal tube, located within the stainless-steel tube, was calibrated by the customer. The concentration of the gas to be generated could be adjusted by regulating the temperature and flow of the system. The formula utilized for this calculation is provided below:

$$Concentration(ppb) = 1000 \cdot Permeation\ Rate\left(\frac{ng}{min}\right) \cdot \frac{\frac{Molecular\ Volume\left(\frac{dm^3}{mol}\right)}{Molecular\ Weight\left(\frac{g}{mol}\right)}}{Sample\ Flow\left(\frac{ml}{min}\right)} \cdot \frac{Sample\ Flow\left(\frac{ml}{min}\right)}{Sample\ Flow\left(\frac{ml}{min}\right) + Split\ Flow\left(\frac{ml}{min}\right)}$$

The formula used to calculate the Permeation Rate, which can be adjusted at various temperatures, is as follows:

$$PermeationRate\left(\frac{ng}{min}\right) = 10\hat{\left(loge - 2950 \cdot \left(\frac{1}{Temperature\ Setpoint(^{\circ}C) + 273} - \frac{1}{Calibration\ Temperature(^{\circ}C) + 273}\right)\right)}$$

The temperature of the permeation tube was set to 85 °C to generate DMMP at a permeation rate of 1042 ng/min. With that, 2.1 ppm are generated, which corresponds to the maximum concentration tested. Subsequently, the generated flow with DMMP is diluted with synthetic dry air, setting an overall and constant flow rate of 100 mL/min.

3. Results and discussion

The Mo_6@Graphene material was prepared by mixing the crystalline $[Mo_6I^i_8(OH)^a_4(H_2O)^a_2]\cdot 2H_2O$ (Mo_6) material and graphene precursors, with a 5% wt loading of the cluster-based material [23]. The sensing performance of the Mo_6@Graphene film for detecting DMMP was assessed at room temperature, leading to low power consumption. Concentrations ranging from 600 ppb to 2.1 ppm of the simulant nerve agent were applied for 5 min, followed by dry air for 15 min to recover the baseline resistance. Fig. 2a illustrates the electrical responses obtained, revealing fast and sensitive responses to DMMP while achieving almost full recovery of the sensor baseline in 15 min. These results are of paramount importance since the Mo_6@Graphene film can detect DMMP in a reversible way, ensuring the sensor's repeatability and stability over time. Furthermore, Fig. S2 illustrates that Mo_6@Graphene maintains its stability even after 24 h of exposure to 2.1 ppm of DMMP. This finding aligns with prior research, where gases like NO_2 and NH_3 did not degrade this nanohybrid [23].

Considering the resistance changes obtained, the sensor response was defined as $\Delta R/R_0$ expressed in percentage, where R_0 is the baseline resistance under synthetic air, and ΔR is the resistance change due to DMMP adsorption. Fig. 2b depicts the calibration curve for detecting

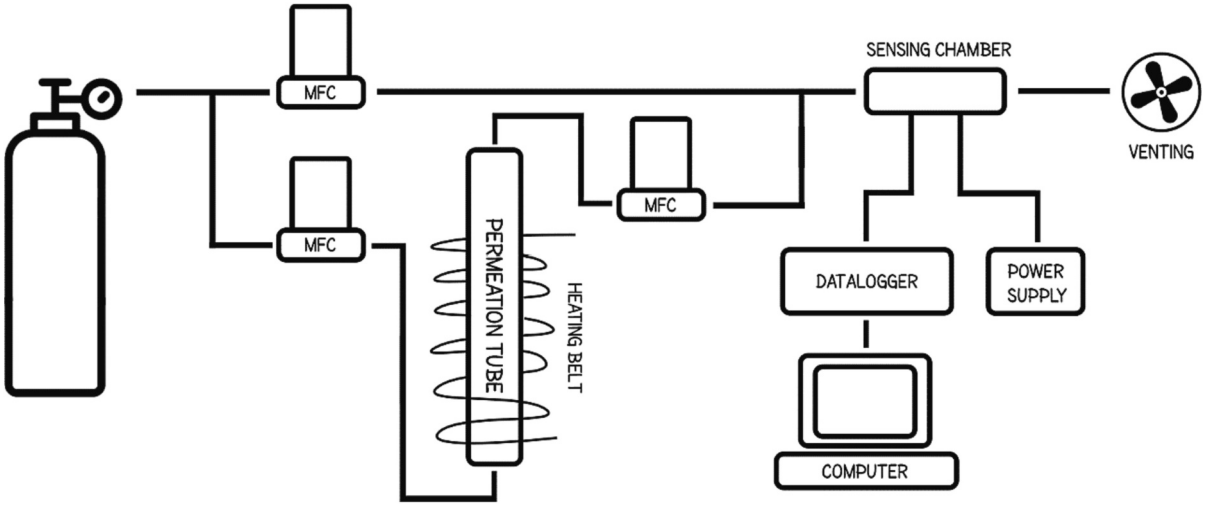

Fig. 1. Diagram of the system used to generate different DMMP concentrations diluted with synthetic air.

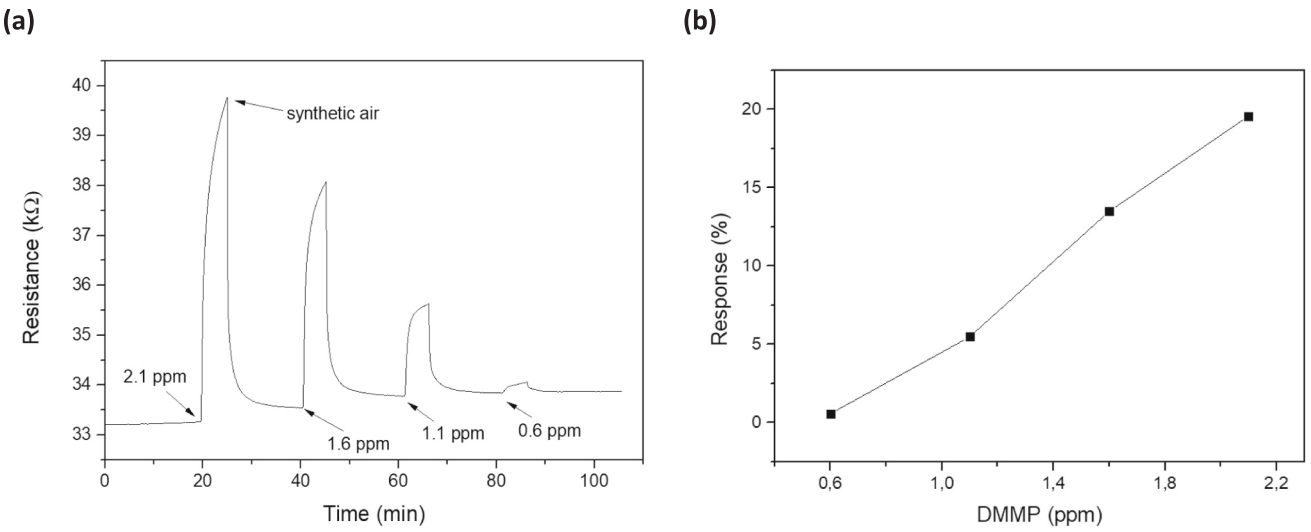

Fig. 2. (a) Electrical responses when using Mo_6@Graphene for detecting DMMP under room temperature conditions, with concentrations ranging from 0.6 to 2.1 ppm. (b) Calibration curve obtained for the different DMMP concentrations measured.

Table 1
Comparison of graphene-based resistive gas sensors for detecting DMMP at room temperature.

Material	Exposure time (s)	Response / Concentration	DMMP concentration range tested	Reference
Mo_6@Graphene	300	5.5% / 1.1 ppm	0.6 – 2.1 ppm	This work
p-phenylenediamine RGO	1080	8% / 20 ppm	5 – 80 ppm	[37]
RGO	150	25% / 10 ppm	10 – 60 ppm	[38]
$r(GO/rGO)_{12}$ multilayers	240	2.21% / 1 ppm	1 – 50 ppm	[39]
PANI/copoly/graphene	120	6.5% / 300 ppb	3 ppb – 30 ppm	[40]
N-substituted triphenylene graphene	Injected by a syringe	0.1% / 1.3 ppm	1.3 ppm	[32]
CoPc-graphene quantum dots	600	9.3% / 20 ppm	20 ppm	[41]
Graphene (UV illuminated)	600	0.5% / 4 ppm	0.8 – 38 ppm	[42]
PPy@Graphene	300	7.5%/1.1 ppm	0.6 – 2.1 ppm	[43]
PPy/rGO	100	3.3% / 5 ppm	5 – 100 ppm	[14]
Cu-N_5 sites PPy/rGO	Injected by a syringe	0.8% / 2 ppm	2 – 100 ppm	[44]
N-carbon nanoparticles and copper ion on rGO	200	10.2% / 100 ppm	10 – 100 ppm	[45]
HFIP-PPy-rGO	144	12.5% / 100 ppm	5–100 ppm	[46]

DMMP at room temperature. It is worth noting that while there might be weak interactions between graphene and DMMP, these would be significantly lower compared to the reactivity of Mo_6 clusters. This assertion is backed by previous research where graphene decorated with Mo_6 demonstrated significantly better sensing performance. The sensitivity is determined by the slope of the calibration curve. Based on the data presented in Fig. 2b, the sensitivity value is calculated as 13% response per ppm of DMMP.

DMMP is a well-known electron donor molecule [32], and its adsorption on the sensor surface results in a transfer of electrons, reducing the hole concentration. When graphene undergoes partial oxidation, it exhibits a mild p-type semiconductor behavior, meaning that holes become the majority carriers. Recently, the electrical response of Mo_6@graphene to NO_2 was demonstrated to mainly result from the incorporation of the Mo_6 cluster material onto graphene. The nanomaterial showed low sensitivity to ammonia, a property tentatively attributed to charge compensation within the ammonia-Mo_6-graphene system [23]. Given the lower Lewis basicity of DMMP compared to ammonia, it is reasonable to expect an increase in the resistive response of the Mo_6@Graphene film upon exposure to DMMP. Consequently, it is reasonable to expect that the electrical resistance of the Mo_6@Graphene film will increase when exposed to DMMP. It is also worth noting the excellent signal-to-noise ratio of the Mo_6@Graphene sensitive film, allowing for a reliable estimation of the limit of detection (LOD) for DMMP. A linear regression was applied to the calibration curve in Fig. 2b to estimate the LOD using the following formula:

$$LOD = 3S_a/b$$

where S_a and b correspond to the standard deviation of y-intercepts and the slope of the regression, respectively. This method resulted in an experimental LOD value of 270 ppb, which is likely lower than that of similar nanomaterials reported previously. Table 1 summarizes the main sensing parameters for detecting DMMP using graphene-based resistors at room temperature conditions, demonstrating the outstanding sensing performance of the Mo_6@Graphene film. The present work represents the first use of a hybrid containing a cluster for detecting this simulant nerve agent. Comparing the sensing performance summarized in Table 1 with similar studies utilizing graphene-based sensors for DMMP detection at room temperature highlights the exceptional performance of Mo_6@Graphene. The concentration of DMMP employed for our measurements is among the lowest reported. More notably, the sensitivity of Mo_6@Graphene, expressed as the response per unit concentration, outperforms most comparable works. However, technology relying on chemiresistive sensors needs further refinement to meet the requirements for real-world applications. Table S1 provides a summary of the limit concentrations for exposures of 10 and 60 min, as per the guidelines established by the National Institute for Occupational Safety and Health (NIOSH) in the United States [33]. However, further studies conducted under humid conditions are necessary to understand the impact of ambient moisture on the sensing performance. Most of the works summarized in Table 1 have not assessed the influence of water molecules on the sensing mechanisms when detecting DMMP. It is worth

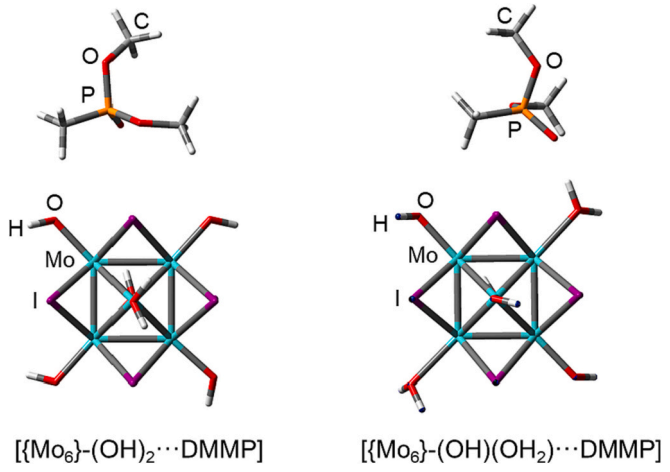

Fig. 3. Representation of the most stable $[Mo_6I^i_8(OH)^a_4(H_2O)^a_2]\cdots$DMMP models (color code: Mo, blue; I, purple; P, orange; O, red; C, grey; H, white). (For interpretation of the references to color in this figure legend, the reader is referred to the web version of this article.)

noting that the volatility of DMMP is heavily affected by ambient moisture, which serves as a significant interferent. An alternative approach could involve using humidity filters to significantly reduce their potential interfering effects [34]. In terms of selectivity, future studies are essential to accurately determine DMMP in complex gas mixtures containing potential interferent gases. The well-known selectivity issues associated with resistive gas sensors require focused efforts on integrating multiple sensors within an array, each with distinct cross-sensitivities [35]. Subsequently, multivariate analysis methods can be employed to discriminate gases in mixtures and to predict gas concentrations [36]. It is important to note that while this approach significantly enhances selectivity, it also leads to increased device complexity and costs.

The robustness of Mo_6@Graphene towards DMMP was assessed by X-ray diffraction, Raman and XPS. After DMMP exposition, the X-ray diffraction and Raman spectra of the nanomaterial do not change (Fig. S2), which indicates that the characteristic crystallinity and composition of the supported Mo_6 material is preserved, and demonstrate the inertness of the graphene support towards DMMP. The Mo3d region of the XPS spectrum (Fig. S5) shows that the binding energies (BEs) obtained at 228.7 eV for $Mo3d_{5/2}$, and 231.9 eV for $Mo3d_{3/2}$ correspond to Mo^{2+} cluster species, accordingly to the electron count of octahedral molybdenum $\{Mo_6I^i_8\}^{4+}$ cluster cores. Similar BEs were found in the literature for analogous $Mo_6X^i_8$ (X^i = halogen) cluster compounds deposited onto carbon surfaces [47–50]. In consequence, the electronic properties of the deposited molybdenum cluster material are preserved after DMMP exposition.

The electrical response observed is mainly attributed to the interaction between DMMP and the $[Mo_6I^i_8(OH)^a_4(H_2O)^a_2]$ cluster model, which was analyzed by DFT studies. Two different orientations (Fig. 3) supramolecular interactions were found between the apical ligands of the cluster compound and the functional groups of the DMMP. The $[\{Mo_6\}\text{-}(OH)_2\cdots DMMP]$ adduct (Fig. 3, left), an interaction between the $–OCH_3$ or $–CH_3$ groups and the oxygen atom of the Mo-OH group is involved, whereas the $[\{Mo_6\}\text{-}(OH)(OH_2)\cdots DMMP]$ adduct (Fig. 3, right) shows Brønsted acid coordination involving Mo-(HOH)···O=P. Calculated BEs increase from −10.3 to −18.5 kcal·mol^{-1}, respectively, and indicate that the formation of cluster-DMMP molecule adducts is exothermic with good agreement with H-bonding interactions. The $[\{Mo_6\}\text{-}(OH)(OH_2)\cdots DMMP]$ adduct is the most energetically stable and this is referred to its shortest interaction, with a P=O···H interatomic length of 1.621 Å. For the same adduct, the DMMP methyl group interacts with the vicinal –OH apical ligand by 2.870 Å. In the case of $[\{Mo_6\}\text{-}(OH)_2\cdots DMMP]$, the H atoms of the methyl and methoxy groups interact with the hydroxo ligands by 2.233 and 2.423 Å, respectively. Thus, the target molecule is likely to be adsorbed reversibly onto the surface of the Mo_6 crystalline material. The proposed sensing mechanism in this study (Fig. S6), considering the physisorption of DMMP onto metal cluster sites, closely resembles the mechanism recently described for the system involving ammonia as a donor molecule [23]. However, a key distinction lies in the reduction of carriers to a lesser extent for the DMMP.

4. Conclusions

The development of detection systems can be used to monitor the environment for the presence of nerve agents, allowing for early detection and a rapid response. In the event of an attack, first responders can use this information to implement appropriate measures to protect the population and mitigate the effects of the attack. In this perspective, the Mo_6@Graphene sensor demonstrated high sensitivity and stability in detecting DMMP at trace levels within a few minutes. The excellent signal-to-noise ratio of the Mo_6@Graphene film enabled the estimation of a low limit of detection (LOD) of 270 ppb, surpassing the performance of similar nanomaterials reported previously. The robustness of the Mo_6@Graphene film was confirmed by X-ray diffraction and XPS analyses. Besides, DFT studies indicate that DMMP chemically adsorbs onto Mo_6 clusters through H-bonding interactions. In summary, the low LOD and fast response time make the Mo_6@Graphene sensor a promising candidate for practical applications in defense and environmental monitoring.

Author contributions

J.C.-C., X.B., R.G.-A., A. M., P.A., E.L., and M.F. conceived and planned the experiments. R.G.-A., A. M. and M.F. carried out the cluster and hybrid materials synthesis and characterizations. J.C.-C. and X.B. carried out the resistive measurements. J.C.-C. performed the resistive data analysis and wrote the first draft. M.F. performed the DFT calculations. M.F. and E.L. supervised the work. All the authors wrote and revised the manuscript. All the authors provided critical feedback and helped shape the research. All the authors have given approval to the final version of the manuscript.

Declaration of Competing Interest

The authors declare that they have no known competing financial interests or personal relationships that could have appeared to influence the work reported in this paper.

Data availability

Data will be made available on request.

Acknowledgments

J.C.-C. is supported by the Marie Skłodowska-Curie Postdoctoral Fellowship (Horizon Europe Programme) under grant agreement No. 101066282 “GREBOS”. E.L. is supported by the Catalan Institute for Advanced Studies (ICREA) via the 2018 Edition of the ICREA Academia Award. This work was supported in part by the Marie Skłodowska-Curie Action (MSCA) Research and in part by the Innovation Staff Exchange (RISE) under Grant no. H2020-MSCA-RISE-2018-823895 “SENSOFT.” This research was also funded by the ITQ though the project PID2021-123163OB-I00 funded by MCIN/AEI/10.13039/501100011033/ and FEDER A way of making Europe and Severo Ochoa centre of excellence program (CEX2021-001230-S). We also thank Dr. Mercedes Boronat for providing us the computational resources at ITQ.

Appendix A. Supplementary data

Supplementary data to this article can be found online at https://doi.org/10.1016/j.sbsr.2023.100603.

References

[1] L. Karalliedde, H. Wheeler, R. Maclehose, V. Murray, Possible immediate and long-term health effects following exposure to chemical warfare agents, Public Health 114 (2000) 238–248.
[2] J. Tafuri, J. Roberts, Organophosphate poisoning, Ann. Emerg. Med. 16 (1987) 193–202.
[3] M. Shaik, V.K. Rao, G.V. Ramana, M. Halder, P.K. Gutch, P. Pandey, R. Jain, P - hexafluoroisopropanol phenyl functionalized graphene for QCM based detection of dimethyl methylphosphonate, a simulant of the nerve agent sarin, RSC Adv. 8 (2018) 8240–8245.
[4] J.B. Decoste, G.W. Peterson, Metal-organic frameworks for air purification of toxic chemicals, Chem. Rev. 114 (2014) 5695–5727.
[5] S.L. Bartelt-Hunt, D.R.U. Knappe, M.A. Barlaz, A review of chemical warfare agent simulants for the study of environmental behavior, Crit. Rev. Environ. Sci. Technol. 38 (2008) 112–136.
[6] D.E. Tevault, J.H. Buchanan, L.C. Buettner, Ambient volatility of DMMP, Int. J. Thermophys. 27 (2006) 486–493.
[7] Y.W. Kuo, C.L. Li, J.H. Jhang, S. Lin, Design of a wireless sensor network-based IoT platform for wide area and heterogeneous applications, IEEE Sensors J. 18 (2018) 5187–5197.
[8] S. Zhuiykov, Mathematical model of electrochemical gas sensors with distributed temporal and spatial parameters and its transformation to models of the real YSZ-based sensors, Ionics (Kiel). 12 (2006) 135–148.
[9] Y. Jian, W. Hu, Z. Zhao, P. Cheng, H. Haick, M. Yao, W. Wu, Gas sensors based on chemi-resistive hybrid functional nanomaterials, Nano-Micro Lett. 121 (12) (2023) 1–43.
[10] K. Kim, O.G. Tsay, D.A. Atwood, D.G. Churchill, Destruction and detection of chemical warfare agents, Chem. Rev. 111 (2011) 5345–5403.
[11] Q. Zheng, Y.C. Fu, J.Q. Xu, Advances in the chemical sensors for the detection of DMMP — a simulant for nerve agent sarin, Procedia Eng. 7 (2010) 179–184.
[12] K. Kacem, J. Casanova-Chafer, S. Ameur, M.F. Nsib, E. Llobet, Gas sensing properties of graphene oxide loaded with SrTiO3 nanoparticles, J. Alloys Compd. 941 (2023), 169011.
[13] J. Casanova-Chafer, R. Garcia-Aboal, P. Atienzar, E. Llobet, Unraveling the gas-sensing mechanisms of lead-free perovskites supported on graphene, ACS Sensors 7 (2022) 3753–3763.
[14] Z. Yang, Y. Zhang, S. Gao, L. Zhao, T. Fei, S. Liu, T. Zhang, Hydrogen bonds-induced room-temperature detection of DMMP based on polypyrrole-reduced graphene oxide hybrids, Sens. Actuators B 346 (2021), 130518.
[15] S. Xu, R. Zhang, J. Cui, T. Liu, X. Sui, M. Han, F. Zheng, X. Hu, Surface acoustic wave DMMP gas sensor with a porous graphene/PVDF molecularly imprinted sensing membrane, Micromachines 12 (2021) 552.
[16] T. Nguyen-Dang, S. Chae, J. Chatsirisupachai, H. Wakidi, V. Promarak, Y. Visell, T. Q. Nguyen, Dual-mode organic electrochemical transistors based on self-doped conjugated polyelectrolytes for reconfigurable electronics, Adv. Mater. 34 (2022) 2200274.
[17] D.J. Osborn, G.L. Baker, R.N. Ghosh, Mo6Cl12-incorporated sol-gel for oxygen sensing applications, J. Sol-Gel Sci. Technol. 36 (2005) 5–10.
[18] J.A. Jackson, M.D. Newsham, C. Worsham, D.G. Nocera, Efficient singlet oxygen generation from polymers derivatized with hexanuclear molybdenum clusters, Chem. Mater. 8 (1996) 558–564.
[19] R.N. Ghosh, G.L. Baker, C. Ruud, D.G. Nocera, Fiber-optic oxygen sensor using molybdenum chloride cluster luminescence, Appl. Phys. Lett. 75 (1999) 2885–2887.
[20] R.N. Ghosh, P.A. Askeland, S. Kramer, R. Loloee, Optical dissolved oxygen sensor utilizing molybdenum chloride cluster phosphorescence, Appl. Phys. Lett. 98 (2011).
[21] M. Amela-Cortes, S. Paofai, S. Cordier, H. Folliot, Y. Molard, Tuned red NIR phosphorescence of polyurethane hybrid composites embedding metallic nanoclusters for oxygen sensing, Chem. Commun. 51 (2015) 8177–8180.
[22] K. Harada, T.K.N. Nguyen, F. Grasset, C. Comby-Zerbino, L. MacAleese, F. Chirot, P. Dugourd, N. Dumait, S. Cordier, N. Ohashi, M. Matsuda, T. Uchikoshi, Light-dependent ionic-electronic conduction in an amorphous octahedral molybdenum cluster thin film, NPG Asia Mater. 141 (14) (2022) 1–9.
[23] J. Casanova-Chafer, R. Garcia-Aboal, P. Atienzar, M. Feliz, E. Llobet, Octahedral molybdenum iodide clusters supported on graphene for resistive and optical gas sensing, ACS Appl. Mater. Interfaces 14 (2022) 57122–57132.
[24] M. Zhang, F. Grasset, Y. Masubuchi, T. Shimada, T.K.N. Nguyen, N. Dumait, A. Renaud, S. Cordier, D. Berthebaud, J.F. Halet, T. Uchikoshi, Enhanced NH3 sensing performance of Mo cluster-MoS2 nanocomposite thin films via the sulfurization of Mo6 cluster iodides precursor, Nanomaterials 13 (2023) 478.
[25] J.P. Perdew, K. Burke, M. Ernzerhof, Generalized gradient approximation made simple, Phys. Rev. Lett. 77 (1996) 3865.
[26] C. Adamo, V. Barone, Toward reliable density functional methods without adjustable parameters: the PBE0 model, J. Chem. Phys. 110 (1999) 6158–6170.
[27] D. Andrae, U. Häußermann, M. Dolg, H. Stoll, H. Preuß, Energy-adjusted ab initio pseudopotentials for the second and third row transition elements, Theor. Chim. Acta 77 (1990) 123–141.
[28] M. Dolg, U. Wedig, H. Stoll, H. Preuss, Energy-adjusted ab initio pseudopotentials for the first row transition elements, J. Chem. Phys. 86 (1987) 866–872.
[29] A. Bergner, M. Dolg, W. Küchle, H. Stoll, H. Preuß, Ab initio energy-adjusted pseudopotentials for elements of groups 13–17, Mol. Phys. 80 (2006) 1431–1441.
[30] A.W. Ehlers, M. Böhme, S. Dapprich, A. Gobbi, A. Höllwarth, V. Jonas, K.F. Köhler, R. Stegmann, A. Veldkamp, G. Frenking, A set of F-polarization functions for pseudo-potential basis sets of the transition metals Sc-Cu, Y-Ag and La-Au, Chem. Phys. Lett. 208 (1993) 111–114.
[31] A. Höllwarth, M. Böhme, S. Dapprich, A.W. Ehlers, A. Gobbi, V. Jonas, K.F. Köhler, R. Stegmann, A. Veldkamp, G. Frenking, A set of D-polarization functions for Pseudo-potential basis sets of the Main group elements Al-Bi and f-type polarization functions for Zn, Cd, Hg, Chem. Phys. Lett. 208 (1993) 237–240.
[32] Y.T. Kim, S. Lee, S. Park, C.Y. Lee, Graphene Chemiresistors modified with functionalized Triphenylene for highly sensitive and selective detection of dimethyl methylphosphonate, RSC Adv. 9 (2019) 33976–33980.
[33] Sarin (GB): Nerve Agent | NIOSH | CDC. https://www.cdc.gov/niosh/ershdb/emergencyresponsecard_29750001.html, 2023 (accessed Oct 27, 2023).
[34] H. Mahdavi, S. Rahbarpour, S.M. Hosseini-Golgoo, H. Jamaati, Reducing the destructive effect of ambient humidity variations on gas detection capability of a temperature modulated gas sensor by calcium chloride, Sens. Actuators B 331 (2021), 129091.
[35] K.J. Albert, N.S. Lewis, C.L. Schauer, G.A. Sotzing, S.E. Stitzel, T.P. Vaid, D.R. Walt, Cross-reactive chemical sensor arrays, Chem. Rev. 100 (2000) 2595–2626.
[36] C. Bur, M. Bastuck, D. Puglisi, A. Schütze, A. Lloyd Spetz, M. Andersson, Discrimination and quantification of volatile organic compounds in the ppb-range with gas sensitive SiC-FETs using multivariate statistics, Sens. Actuators B 214 (2015) 225–233.
[37] N. Hu, Y. Wang, J. Chai, R. Gao, Z. Yang, E.S.W. Kong, Y. Zhang, Gas sensor based on P-phenylenediamine reduced graphene oxide, Sens. Actuators B 163 (2012) 107–114.
[38] T. Alizadeh, L.H. Soltani, Reduced graphene oxide-based gas sensor array for pattern recognition of DMMP vapor, Sens. Actuators B 234 (2016) 361–370.
[39] Y. Wang, M. Yang, W. Liu, L. Dong, D. Chen, C. Peng, Gas sensors based on assembled porous graphene multilayer frameworks for DMMP detection, J. Mater. Chem. C 7 (2019) 9248–9256.
[40] H. Yu, H. Han, J. Jang, S. Cho, Fabrication and optimization of conductive paper based on screen-printed polyaniline/graphene patterns for nerve agent detection, ACS Omega 4 (2019) 5586–5594.
[41] K.T. Alali, J. Liu, R. Chen, Q. Liu, H. Zhang, J. Li, J. Hou, R. Li, J. Wang, HFIP-functionalized Co3O4 Micro-nano-octahedra/RGO as a double-layer sensing material for chemical warfare agents, Chem. – A Eur. J. 25 (2019) 11892–11902.
[42] J. Park, R. Rautela, N. Alzate-Carvajal, S. Scarfe, L. Scarfe, L. Alarie, A. Luican-Mayer, J.M. Ménard, UV illumination as a method to improve the performance of gas sensors based on graphene field-effect transistors, ACS Sensors 6 (2021) 4417–4424.
[43] J. Casanova-Chafer, X. Blanch, E. Llobet, Polypyrrole nanoparticles suspended on graphene for the detection of simulant chemical warfare agents, IEEE Sensors Lett. (2023) 1–4.
[44] Z. Yang, L. Zhao, Y. Zhang, Y. Xing, Z. Wei, C. Xin, T. Fei, S. Liu, T. Zhang, Isolated cu-N5 sites engineered Polypyrrole-reduced graphene oxide hybrids for enhancing room-temperature DMMP sensing, Sens. Actuators B 385 (2023), 133671.
[45] Y. Xing, Z. Yang, L. Zhao, Y. Zhang, Z. Wei, C. Xing, T. Fei, S. Liu, T. Zhang, A multisite strategy to improve room-temperature DMMP sensing performances on reduced graphene oxide modulated by N-doped carbon nanoparticles and copper ions, Sens. Actuators B 393 (2023), 134220.
[46] Z. Yang, Z. Wei, Y. Xing, L. Zhao, Y. Zhang, C. Xin, T. Fei, S. Liu, T. Zhang, Synergy of two intermolecular hydrogen bonds promotes highly sensitive and selective room-temperature dimethyl Methylphosphonate sensing: a case of RGO-based gas sensors, Langmuir 39 (2023) 10935–10946.
[47] P. Kumar, H.P. Mungse, S. Cordier, R. Boukherroub, O.P. Khatri, S.L. Jain, Hexamolybdenum clusters supported on graphene oxide: visible-light induced photocatalytic reduction of carbon dioxide into methanol, Carbon N. Y. 94 (2015) 91–100.
[48] M. Feliz, M. Puche, P. Atienzar, P. Concepción, S. Cordier, Y. Molard, In situ generation of active molybdenum octahedral clusters for photocatalytic hydrogen production from water, ChemSusChem 9 (2016) 1963–1971.
[49] C. Godet, S. Ababou-Girard, B. Fabre, Y. Molard, A.B. Fadjie-Djomkam, S. Députier, M. Guilloux-Viry, S. Cordier, Surface immobilization of Mo6I8 octahedral cluster cores on functionalized amorphous carbon using a pyridine complexation strategy, Diamond Relat. Mater. 55 (2015) 131–138.
[50] A. Barras, M.R. Das, R.R. Devarapalli, M.V. Shelke, S. Cordier, S. Szunerits, R. Boukherroub, One-pot synthesis of gold nanoparticle/molybdenum cluster/graphene oxide nanocomposite and its photocatalytic activity, Appl. Catal. Environ. 130–131 (2013) 270–276.